THE JOURNAL OF PHYSICAL CHEMISTRY B

Article

Cite This: J. Phys. Chem. B 2018, 122, 8796−8804

pubs.acs.org/JPCB

Tests of Kramers' Theory at the Single-Molecule Level: Evidence for Folding of an Isolated RNA Tertiary Interaction at the Viscous Speed Limit

Nicholas F. Dupuis, Erik D. Holmstrom, and David J. Nesbitt*

JILA, University of Colorado and National Institute of Standards and Technology, Department of Chemistry and Biochemistry, and Department of Physics, University of Colorado, Boulder, Boulder, Colorado 80309, United States

Supporting Information

ABSTRACT: Dissipation and friction influence the conformational dynamics of biological polymers as they traverse barriers on rugged free energy surfaces. It is well established that the "speed limit" for macromolecular folding is dictated by a combination of (i) solvent friction, which depends on solvent viscosity, η, and (ii) internal friction, which is independent of solvent and depends solely on the molecular folding pathway. In this work, single-molecule Förster resonance energy transfer (FRET) confocal spectroscopy is used to study viscosity-dependent folding kinetics of an isolated RNA tertiary motif, that of the GAAA tetraloop receptor, allowing both solvent and internal frictional contributions to be investigated and extracted independently for both flexible PEG- and RNA-based (rU7, rA7) linkers in the unimolecular construct. Specifically, our single-molecule data reveal that (i) folding rate constants scale linearly with the inverse solvent viscosity (η), which supports Kramers'/Grote−Hynes' rate theory for η-dependent RNA folding and that (ii) they provide quantitative upper limits for the intrinsic viscosity, [$\eta_{int} \approx 0.1(2)$ cP], arising from internal friction associated with folding/unfolding of an isolated RNA tertiary interaction. Furthermore, in contrast to strong viscosity-induced shifts in the folding/unfolding rate constants, temperature-dependent studies demonstrate that the enthalpic, entropic, and free energy contributions to the transition state barrier are largely insensitive to the solvent viscosity. This supports a very simple picture for the conformational kinetics of isolated RNA tertiary interactions wherein rate constants for folding/unfolding are both inversely dependent on viscosity and limited by diffusional access to the transition state region on a multidimensional free energy surface. Particularly under cellular conditions, where $\eta_{solv} > 1$ cp, this suggests that RNAs fold/unfold at a "speed limit" dictated by solvent viscosity and transition-state barrier thermodynamics rather than internal molecular friction.

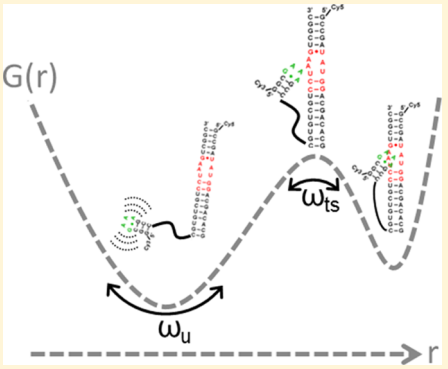

1. INTRODUCTION

In the cell, RNAs fold and unfold continuously in a complex heterogeneous solution containing other macromolecules (e.g., proteins and nucleic acids), inorganics (e.g., K^+, Na^+, Mg^{++}, Cl^-, and HCO_3^-), and small co-solutes (e.g., amino acids, NTPs, cofactors, and vitamins), all of which influence the free energy surface.[1−3] The conformational rearrangements of such a polymer, resulting in folding and unfolding transitions, are thermally driven by Brownian motion and are expected to exhibit diffusive dynamics on a low dimensionality free energy surface (see Figure 1). Because of this diffusive exploration of conformational space, the kinetics of RNA folding/unfolding will naturally depend explicitly on the solvent friction. However, this may not be the only source of dissipation. Internal friction, for example, due to polymer rearrangement on a rough free energy landscape may also affect these dynamical processes, thus slowing the folding kinetics.[4,5] Indeed, for proteins, such polymeric internal chain friction has been shown to present an important limitation (i.e., "speed limit") to the kinetics of conformational transitions.[5−16] By way of contrast, however, relatively little is known about the corresponding solvent and/or internal frictional effects associated with RNA folding.[17] One particularly relevant aspect is that the dynamics of RNA folding are generally found to be hierarchical, with secondary structures (loops and helices) forming on much faster time scales ($\sim 10^{-6}$ s) than tertiary structures (long range loop−loop and loop−helix interactions, $\sim 10^{-3}$ to 10^3 s). In this regard, the role of frictional effects for RNA could be quite different for different aspects of this hierarchy, and in particular, it is currently unclear how solvent friction versus internal friction might contribute to the dynamics of either secondary or tertiary structure formation.

This work systematically explores the influence of solution viscosity on RNA tertiary conformational kinetics at the single-molecule level. Specifically, these studies permit the deconstruction of contributions from both solvent and internal friction in the folding/unfolding of an isolated, single tertiary

Received: April 27, 2018
Revised: August 1, 2018
Published: August 4, 2018

DOI: 10.1021/acs.jpcb.8b04014
J. Phys. Chem. B 2018, 122, 8796−8804

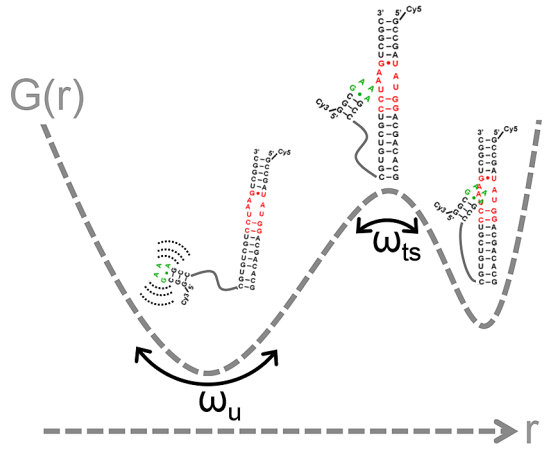

Figure 1. Schematic 1D free energy surface for folding dynamics of single-molecule tetraloop−X−receptor RNA constructs, where X represents a flexible polymer linker of either ethylene glycol, rU, or rA repeat subunits. In the spirit of Kramers' theory, r represents a 1D simplification of a highly multidimensional reaction coordinate describing proximity/orientation between the tetraloop/receptor, with ω_u and ω_{ts} indicating real and imaginary frequencies associated with the unfolded and transition-state geometries, respectively.[18] In Kramers' theory, the GAAA-tetraloop, linker, and receptor moieties diffusively search through a multidimensional rough free energy landscape in order to achieve the requisite transition state conformation, which can give rise to an additional viscosity intrinsic to the polymer construct and further slow down the folding rate processes. This is consistent with the rate constant k scaling inversely with the effective viscosity η_{eff} given by a sum of solvent (η_{solv}) + internal (η_{int}) viscosities of the RNA construct.

interaction (GAAA tetraloop−receptor construct). The theoretical framework for this investigation is based on Kramers' pioneering development of barrier transmission kinetics in a dissipative medium[18] and extensions of this theory by Grote and Hynes[19−23] to incorporate effects due to time/frequency dependent friction and multiple reactive and nonreactive coordinates. In the context of these theories, the rate of passage over a harmonic barrier arises from a particle undergoing Brownian diffusion in a harmonic potential (see Figure 1), which is derived from a multidimensional free energy surface with friction provided by a continuum solvent.[18,24] In this formulation, the rate of folding is given by $k_{fold} = \kappa k^{tst}$, where κ is the transmission coefficient for barrier crossing and k^{tst} is the unimolecular rate constant derived from the transition-state theory [i.e., $k^{tst} = \nu \exp(-\Delta G^{\ddagger}/kT)$]. In this expression, the prefactor, $\nu = \omega/(2\pi)$, is the "attempt frequency" for motion along the reaction coordinate in the vicinity of the reactant minimum, while $\Delta G^{\ddagger}$ represents the transition-state free energy barrier. If one neglects frequency dependence in the solvent friction, the Grote−Hynes expression for κ is given self-consistently by

$$\kappa = 1/(\kappa + [\zeta/\mu\omega_{TST}]) \quad (1)$$

where ζ represents the frequency-independent frictional force per unit velocity, ω_{TST} is the imaginary frequency of the transition state barrier, and μ is the effective mass for progress along the folding coordinate. In the limit of low solvent friction ($\zeta/\mu \ll \omega_{TST}$), eq 1 yields $\kappa^2 \approx 1$, and therefore, one recovers the standard transition-state theory result, that is, $k_{fold} \approx k^{tst}$. Conversely, in the limit of high solvent friction ($\zeta/\mu \gg \omega_{TST}$), the transmission coefficient is predicted to scale inversely with frictional drag ($\kappa \approx \mu\omega_{TST}/\zeta$), which yields a rate constant for folding given by

$$k_{fold} = (\mu\omega_{TST}/2\pi\zeta) \exp(-\Delta G^{\ddagger}/kT) \quad (2)$$

For any quantitative comparison with the experiment, one must also stipulate a connection between the microscopic frictional coefficient (ζ) and macroscopic viscosity (η), which in general will depend on details of a given theoretical model. For example, if we consider the simplest Stokes law treatment for viscous drag on a sphere of effective radius R (i.e., $\zeta = 6\pi R\eta$), the rate constant expression becomes

$$k_{fold} = \kappa k^{tst} = [\mu\omega_{TST}/(12\pi^2\eta R)] \exp(-\Delta G^{\ddagger}/kT) \quad (3)$$

which directly predicts an inverse dependence of folding rates on the solvent viscosity. Simply stated, Kramers' and Grote−Hynes' theory offer, via eq 3, explicit expectations for the viscosity dependence of the elementary rate process in conformational folding/unfolding of RNA, which can be tested by studying the folding kinetics of an isolated RNA tertiary interaction using single-molecule techniques.[9]

As mentioned previously, however, additional dissipative mechanisms may contribute to the folding kinetics, including friction within the polymer chain itself. Indeed, the role of such internal friction in establishing a "speed limit" for protein folding has been well documented, as first demonstrated by Eaton and co-workers,[7,25,26] with major theoretical and experimental contributions by the groups of Szabo, Wolynes, Schuler, Gruebele, Thirumalai, and others.[5,6,12−16,27−36] Since that time, numerous studies have explored effects due to internal friction in polymer folding, with plots commonly made of the relaxation lifetime ($\tau = 1/k$) versus solvent viscosity (η_{solv}).[5−11] In the context of such an analysis, extrapolation of this relaxation lifetime to $\eta_{solv} = 0$ allows one to extract an effective intrinsic viscosity arising from internal friction within the polymer, as well as the time scales for folding at the viscous "speed limit."[5,7,8,10,34,35,37]

In the present work, we directly test Kramers'/Grote−Hynes' theory by applying it to viscosity-dependent RNA folding kinetics measured using single-molecule Förster resonance energy transfer (smFRET). In particular, this analysis is used to extract information on contributions from both solvent and internal friction. First, we find that both k_{fold} and k_{unfold} for three RNA constructs are systematically slowed by increasing viscosity, in agreement with the $1/\eta$ dependence predicted by Kramers'/Grote−Hynes' theory. Second, these viscosity-dependent changes in the forward/reverse rate constants are, within experimental uncertainty, perfectly proportional and in the same direction, which results in a viscosity-independent equilibrium constant, K_{eq}, and folding free energy, ΔG°. Third, the temperature-dependent single-molecule kinetic data reveal that changes in the solvent viscosity influence neither enthalpic nor entropic contributions to the overall folding free energy, but instead simply increase or decrease the frequency with which the RNA attempts to cross the transition state barrier. Finally, we quantify the magnitude of solvent-independent contributions to the folding speed limit by analyzing plots of $1/k$ versus η for the isolated tetraloop−receptor constructs, which indicate negligibly small effects due to internal polymer friction. Most importantly, the absence of an internal "speed limit" for the folding of an isolated RNA tetraloop receptor tertiary interaction establishes

DOI: 10.1021/acs.jpcb.8b04014
J. Phys. Chem. B 2018, 122, 8796−8804

an important precedent and stimulus for future RNA folding studies.

2. MATERIALS AND METHODS

2.1. RNA Construct and Reagents. The isolated GAAA loop−receptor RNA construct is assembled by annealing together three pieces of RNA purchased from IDT (Coralville, IA): (i) a DNA surface tether strand, 5′-biotin-CGC ACT CGT CTG AG-3′, (ii) a Cy5-labeled helix strand, 5′-Cy5-GCC GAU AUG GAC GAC ACG CCC CUC AGA CGA GUG CG-3′, and (iii) a Cy3-labeled tetraloop-linker-helix strand, 5′-Cy3-GGC GAA AGC C-**X**-CGU GUC GUC CUA AGU CGG C-3′, where **X** is a EG_6, rU_7, or rA_7 linker and the subscripts refer to the number of ethylene glycol, rU, and rA subunits. Though the main focus of this work is on the docking/undocking dynamics of the GAAA tetraloop receptor, the use of both polymeric EG_6, rU_7, or rA_7 and RNA-based (rU7 and rA7) linkers permits us to additionally explore the influence of a flexible, nonbiochemical versus ribonucleic acid linker on the viscosity-dependent folding dynamics. The three assembled constructs (TLR1, TLR2, and TLR3 for X = EG_6, rU_7, or rA_7, respectively) have been used directly without further purification. Figure 2 shows the sequence, secondary and likely tertiary structure of the FRET-labeled constructs with a TLR1 (i.e., EG_6) linker.

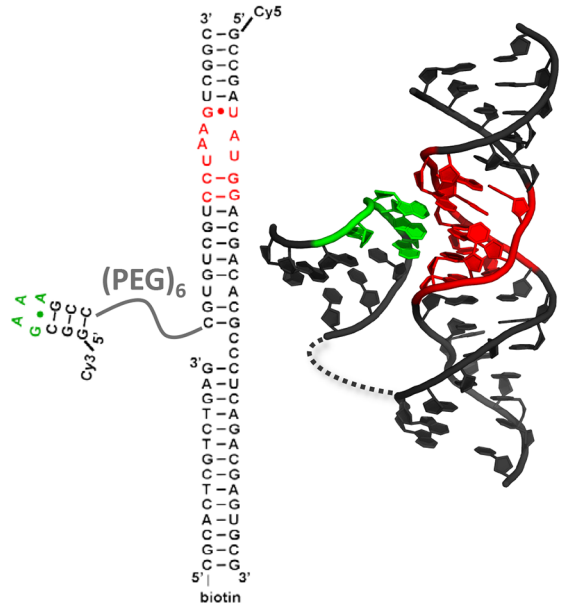

Figure 2. Schematic of the three-strand construct (with X = EG_6) designed to explore viscosity-dependent folding and unfolding in an isolated tetraloop−receptor tertiary interaction in a single RNA. The left-hand side illustrates the secondary structure of the unfolded state, with the approximate folded 3D structure of the tetraloop−receptor tertiary interaction shown in the right-hand side. This 3D structure also highlights the greater proximity of the donor and acceptor moieties and the increase in the E_{FRET} value achieved upon folding.

Samples are prepared for imaging by creating a channel between two pieces of a double-sided tape, sandwiched by a glass slide and a methanol-cleaned coverslip. The channel is flushed with a 10:1 mixture of BSA/BSA-biotin at ∼1 mg/mL total protein concentration, followed by streptavidin (∼0.1 mg/mL), and lastly, an RNA construct at ∼100 pM dilution. To image, the sample is flushed with a solution that contains the following: (i) 50 mM HEPES buffer (pH 7.5), (ii) 100 mM NaCl and 0.1 mM EDTH, (iii) 2 mM Trolox (9-hydroxy-2,5,7,8-tetramethylchroman-2-carboxylic acid), (iv) ∼0.1 mg/mL protocatechuate 3,4-dioxygenase, ∼10 mM 3,4-dihydroxybenzoic acid to catalytically remove oxygen, and (v) glycerol (0−50 v/v % with in 50 mM buffer) to achieve the desired solution viscosity.

2.2. Confocal Imaging. The surface-immobilized molecules are imaged with a home-built confocal microscope that has been described in detail elsewhere.[38,39] The samples are illuminated with 532 nm light from a pulsed Nd:YAG laser focused to a diffraction-limited spot by a 1.2 NA water immersion objective. The fluorescence from single dye-labeled RNAs is collected through the same objective, focused through a 50 μm pinhole and split by both polarization and color into donor (Cy3) and acceptor (Cy5) channels with dichroic mirrors (645 nm) prior to being detected on separate avalanche photodiodes, where the arrival time of every photon is recorded using time-correlated single photon counting methods. Background correction, calculation of E_{FRET}, and analysis of the dwell time distributions are performed with software written in-house. For each rate constant measurement, E_{FRET} trajectories for this exclusively 2-state folding system are analyzed by establishing a threshold between high and low E_{FRET} states. The time duration a molecule spends in each state (i.e., τ_{fold} or τ_{unfold} "dwell times") is tabulated and integrated to generate cumulative distribution functions (CDFs) that describe the probabilistic decay from one state into the other. These CDFs are well described by a single exponential function, fits to which yield k_{fold} and k_{unfold}, respectively. For temperature-dependent measurements, the microscope stage and objective are both heated to a desired temperature (20−35 ± 0.5 °C) using commercially available heaters with PID servo loop control.[40,41]

One important concern is whether the tethering of the RNA constructs to the coverslip surface might interfere with the folding dynamics and energetics. By way of testing for (and ruling out) such effects, we have performed multiple single-molecule studies of this tetraloop receptor construct, as a function of monovalent (Na^+ and K^+), divalent (Mg^{2+} and Mn^{2+}), and trivalent ion (Fe^{3+}) concentrations,[42,43] as well as a function of different flexible tether composition/length choices and temperature conditions.[40,44,45] In no case have we seen evidence for effects on the unimolecular rate or equilibrium constants due to the choice of surface immobilization. We have also extensively tested our constructs using single-molecule burst methods under freely diffusing conditions, which eliminates the surface tethering process entirely.[39] Most importantly, the burst methods permit us to measure the equilibrium constants directly, which are in excellent agreement with the ratio of the rate constants measured under tethered conditions.

3. RESULTS

3.1. Folding Kinetics for RNA Tertiary Structure Formation Depends Strongly on Viscosity. We first explore the folding kinetics in the absence of additional viscogen. As shown in Figure 3 (upper panel), we plot the temporal evolution of the red (acceptor) and green (donor) photon arrivals, summed into 8 ms bins. These red/green intensity ratios can be readily converted into a time-dependent E_{FRET} value, as plotted in the middle panel of Figure 3. Most importantly, the time-dependent E_{FRET} values demonstrate a

DOI: 10.1021/acs.jpcb.8b04014
J. Phys. Chem. B 2018, 122, 8796−8804

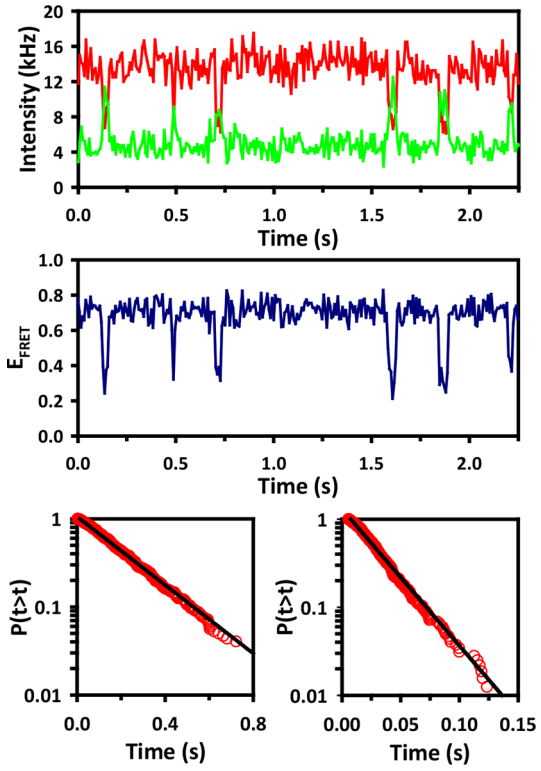

Figure 3. Sample single-molecule data for folding/unfolding episodes in the tetraloop−EG_6−receptor (TLR1) construct in the absence of added glycerol. The binned intensities of donor (green) versus acceptor (red) photon counts are shown versus time in the upper panel, with the corresponding E_{FRET} trajectory plotted versus time in the middle panel, which indicate clear switching between a low and high FRET state. Log-linear plots of the cumulative probability distributions for the folding and unfolding dwell times are summarized in lower left and right panels, respectively. The single exponential nature of these plots is indicative of the two-state folding nature of the tetraloop−receptor construct.

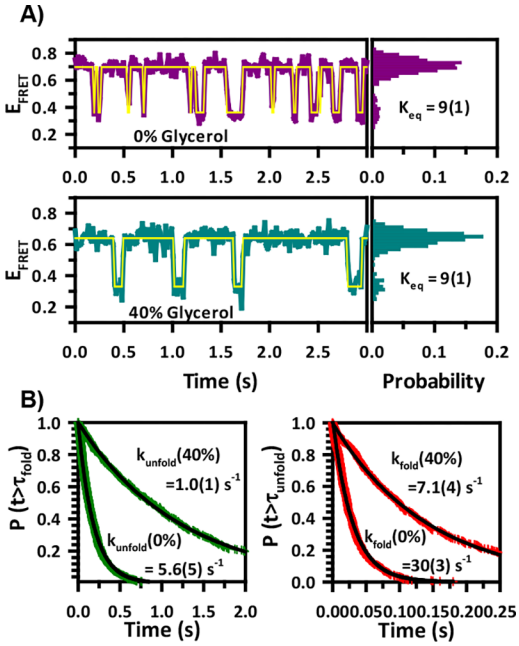

Figure 4. (A) Sample E_{FRET} trajectory data for binary folding/unfolding kinetics of the TLR1 (X = EG_6) construct, which clearly reveal a dramatic slowing with increasing glycerol fraction. Time-integrated histograms of these trajectories (right side of panel A) reveal only negligible changes in K_{eq}, which implies $\Delta\Delta G^\circ \approx 0$, that is, no preferential interactions between glycerol and the folded/unfolded conformations of the RNA. (B) CDFs for folded/unfolded dwell times indicate simple unimolecular exponential decay kinetics. Note that both folding/unfolding rate constants decrease by the same factor with added glycerol, which allows $K_{eq} = k_{fold}/k_{unfold}$ to remain constant, as evident in the right-most panels of (A).

clear two-state switching behavior between high and low FRET values, with the distribution of time windows consistent with conversion between folded and unfolded states occurring on the 10−100 ms time scale. This is demonstrated more quantitatively in kinetic plots of the cumulative probability distributions versus time (lower panel, Figure 3), which reveal purely single exponential decays in both the folding and unfolding directions.

With two-state folding behavior clearly established, the effect of solvent viscosity on the folding and unfolding kinetics of these RNA constructs has been systematically explored by adding glycerol to aqueous solutions.[46] Sample E_{FRET} trajectories for the tetraloop−EG_6−receptor construct (i.e., TLR1) are shown in Figure 4A for 0 and 40% glycerol by volume (v/v). Relative to pure aqueous conditions, the dwell times in both the folded (τ_{fold}, E_{FRET} = 0.7) and unfolded (τ_{unfold}, E_{FRET} = 0.3) conformations increase with glycerol fraction, corresponding to a decrease in both k_{unfold} and k_{fold}, respectively. Despite this strong sensitivity in the folding/unfolding dwell times to viscosity, it is worth noting that the cumulative FRET histograms derived from these trajectories (rightmost panel, Figure 4A) exhibit negligible change in the equilibrium constant [$K_{eq} \approx 9(1)$] over the full range of glycerol conditions. A similar insensitivity in K_{eq} to solution viscosity has also been demonstrated in Figure S1 for single-molecule GAAA tetraloop receptor constructs with the biochemically more relevant nucleic acid linkers (rU_7 and rA_7). This is consistent with predictions from Kramers' and Grote−Hynes' theory, whereby viscous drag in the high friction limit slows diffusional access to the transition state without influencing the relative stabilities of "reactants" (unfolded) and "products" (folded).

A more quantitative illustration of how glycerol alters the folding rate constants is shown by CDFs in Figure 4B. Such CDFs describe the decay from one state into the other, with the rate constants for folding and unfolding determined by single exponential fits to the τ_{unfold} and τ_{fold} CDFs, respectively. For example, the addition of 40% glycerol extends the CDFs for the TLR1 construct (X = EG_6) to significantly longer time scales (see Figure 4, lower right). This dramatic slowing of the kinetics is summarized in Figure 5, where k_{fold} and k_{unfold} for the TLR1 constructs are plotted as a function of glycerol volume fraction (v/v). In both folding and unfolding directions, the rate constants systematically decrease with increasing glycerol volume fraction and thus solution viscosity. It is worth noting for later discussion that the dashed gray lines are not least-squares fits to the data, but rather represent simple predictions from Kramers'/Grote−Hynes theory corresponding to an exact $1/\eta$ scaling of the normalized rate constants with respect to the solution viscosity.[9,18,46]

This analysis can be taken one step further in Figure 6 by calculating (i) equilibrium constants (K_{eq}, red circles, left hand side) and (ii) folding free energies [$\Delta G^\circ = -RT \ln(K_{eq}/K_{eq}^\circ)$, blue circles, right hand side] at each glycerol volume fraction.

DOI: 10.1021/acs.jpcb.8b04014
J. Phys. Chem. B 2018, 122, 8796−8804

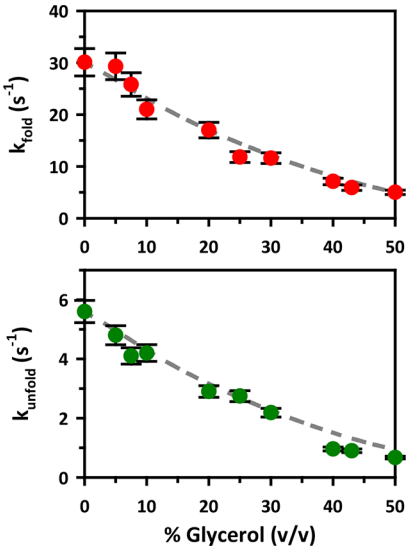

Figure 5. Dependence of the unimolecular rate constants for folding (upper panel) and unfolding (lower panel) of the tetraloop–EG_6–receptor (TLR1) construct on the glycerol concentration. Predictions from Kramers' and Grote–Hynes' theory in the high friction limit (i.e., k proportional to $1/\eta$) are shown with dashed gray lines, which capture the experimentally observed behavior with quantitative accuracy. The data are consistent with a strong but nearly perfectly balanced decrease in the rate constants with increasing solvent viscosity, which allows the equilibrium constant (K_{eq}) to remain constant, as indicated in Figure 4. Similar glycerol-dependent data for the full series of RNA constructs can be found in the Supporting Information (Figures S1 and S2).

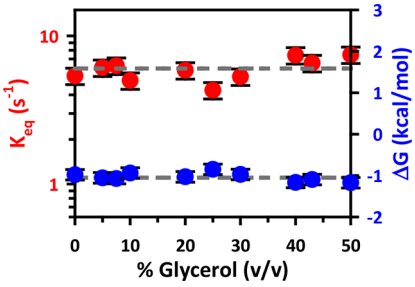

Figure 6. Plots of the RNA folding/unfolding equilibrium constants (K_{eq}, red circles, left) and the overall free energy changes ($\Delta G°$, blue circles, right) as a function of the glycerol concentration for the TLR1 construct. The flatness of the lines for both K_{eq} and $\Delta G°$ indicate negligible shifts in the overall free energy for folding with added glycerol. Note that this does not imply a complete lack of interaction between glycerol and RNA, but simply that the shifts must be equivalent for both the folded vs unfolded states of the RNA construct. Similar glycerol-dependent K_{eq} and $\Delta G°$ data for the series of RNA constructs can be found in the Supporting Information (Figure S1B,C).

As noted in the abovementioned discussion, both of these physical parameters should be independent of solution viscosity in the high friction limit of Kramers'/Grote–Hynes' theory. Indeed, although the K_{eq} values vary by more than an order of magnitude between the three different RNA constructs [see Figure S1 for summary data on each of the X = EG_6, rU_7, and rA_7 (TLR1,2,3) constructs], the glycerol dependences for each construct are very well described by horizontal lines with zero slope and largely independent of the biochemical (rU_7 and rA_7) versus nonbiochemical (EG_6) nature of the linker. Similarly, the glycerol-dependent plot of $\Delta G°$ in Figure 6 (blue circles) clusters around a constant value, again in good agreement with theoretical predictions. In summary, the single-molecule kinetic data are consistent both with (i) the predictions from the high friction limit of Kramers' and Grote–Hynes' theory (eqs 1–3) and (ii) the viscosity-independent equilibrium E_{FRET} histograms in Figure 4A.

3.2. RNA Folding Speed Limits by Solvent and Internal Friction. The $1/\eta$ scaling of the rate constants due to solvent friction (ζ_{solv}) and viscosity (η_{solv}) is consistent with Kramers' theory and provides support for a simple physical picture of 1D diffusive molecular motion across a barrier derived from a free energy surface with many more degrees of freedom. However, the intrinsic viscosity (η_{int}) resulting from internal friction (ζ_{int}) within the RNA polymer chain might also be expected to slow folding/unfolding kinetics. To explore such effects, we specifically define the "effective viscosity" as the sum of solvent and intrinsic contributions ($\eta_{eff} = \eta_{solv} + \eta_{int}$) and argue from Kramers' theory that the experimental rate constant k_{exp} for folding/unfolding should also scale inversely with this effective viscosity for the experimental process. This implies

$$\tau_{exp} = 1/k_{exp} = C\eta_{eff} = C\{\eta_{solv} + \eta_{int}\} \quad (4)$$

where the constant of proportionality is $C = (12\pi^2 R/\mu\omega_{TST})\exp(\Delta G^{‡}/kT)$. As predicted from eq 4, a plot of $1/k_{exp}$ versus η_{solv} should therefore yield a straight line with slope, m, and intercept, $m\eta_{int}$, with an intercept/slope ratio ($m\eta_{int}/m = \eta_{int}$) corresponding to the intrinsic viscosity arising from internal friction within the RNA construct. Such analyses of the folding and unfolding kinetic data for the TRL1 (X = EG_6) construct are displayed in the upper and lower panels of Figure 7, respectively, with the full set of kinetic data for all three linker constructs summarized in Figure S2. Least-squares fits of k_{fold} versus $1/\eta$ data yield a series of straight lines that pass through the origin and are consistent with a negligible intrinsic viscosity. A more quantitative estimate of these intrinsic viscosities is obtained from the intercept/slope ratios, which are all experimentally indistinguishable from zero within uncertainty and yield $\eta_{int} = -0.16(25)$, $0.11(25)$, and $-0.09(25)$ cP for linkers X = EG_6, rU_7, or rA_7, respectively. This implies that the folding and unfolding rate constants for a simple yet biologically ubiquitous RNA tertiary interaction must be dominated by solvent viscosity, with negligible contributions due to internal friction arising from the intrinsic molecular properties of the construct and the adjoining linker. Alternatively stated, the folding/unfolding kinetics are well described by Kramers'/Grote–Hynes' theory, with a kinetic "speed limit" dominated by solvent friction in any solution with a solvent viscosity in excess of $\eta_{int} \approx 0.1(2)$ cP. This condition is certainly satisfied, for example, in the cellular cytoplasm, because water at room temperature already has a viscosity of $\eta_{aq} \approx 1.0$ cP even in the absence of contributions due to added solute.[47]

3.3. Temperature-Dependent Viscosity Effects. As demonstrated above, increasing concentrations of glycerol induce significant shifts in both the folding and unfolding rate constants for the ubiquitous tetraloop receptor RNA tertiary interaction, which counterbalance each other so as to maintain the same free energy difference ($\Delta G°$) and the overall equilibrium constant. For additional insight into the underlying thermodynamics, we have determined these kinetic and equilibrium RNA folding properties over a range of temper-

DOI: 10.1021/acs.jpcb.8b04014
J. Phys. Chem. B 2018, 122, 8796–8804

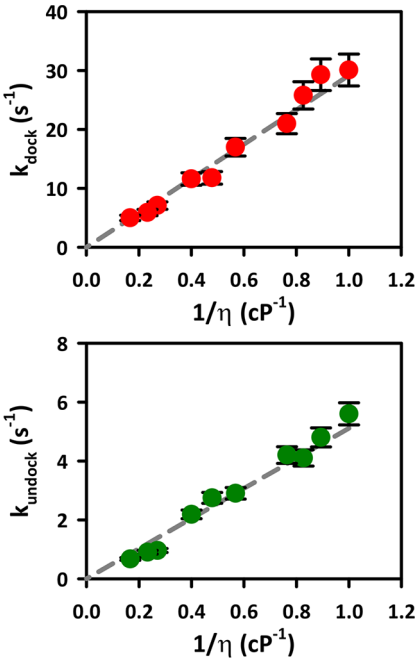

Figure 7. Kinetic plots of the folding (upper panel) and unfolding (lower panel) unimolecular rate constants for the TLR1 construct as a function of the inverse solvent viscosity. From Kramer's and Grote–Hynes' theory in the high friction limit, such a plot should reveal contributions due to intrinsic friction of the polymer (η_{int}) given by the slope to intercept ratio. The excellent linear fits to the data with zero intercepts (gray dashed lines) indicate that the intrinsic friction for this construct is zero within experimental uncertainty. Similar data for the full series of RNA constructs can be found in the Supporting Information (Figures S1A and S2).

atures in either pure aqueous or water–glycerol solutions. Most critically, such temperature-dependent experiments permit one to deconstruct both the overall and transition-state free energies each into corresponding entropic and enthalpic contributions. By way of example, Figure S3 displays a van't Hoff plot of $\ln(K_{eq})$ versus $1/T$ for TLR1 at 0, 30, and 50% glycerol, for which the slope $(-\Delta H^{\circ}/R)$ and intercept $(\Delta S^{\circ}/R)$ reflect the overall enthalpic and entropic differences associated with the conformational equilibrium. Fits to the three data sets yield the same slopes within the experimental error, consistent with an exothermic release of heat ($\Delta H^{\circ} \approx -23(2)$ kcal/mol) upon folding, which is partially offset by a negative change in entropy ($\Delta S^{\circ} \approx -70$ to -79 cal/mol·K). The observed exothermicity is quite reasonable based on an overall formation of multiple hydrogen bonds and stacking interactions in the tetraloop–receptor tertiary construct. Similarly, the negative entropy change is consistent with a greater ordering in the folded tetraloop receptor construct versus the dissociated unfolded tetraloop and receptor moieties. These thermodynamic values also agree with previous studies of the tetraloop–receptor construct ($\Delta H^{\circ} = -23.9(9)$ kcal/mol, $\Delta S^{\circ} = -80(3)$ cal/mol·K) measured under similar solution conditions.[41,43,45]

To extract additional information on the transition-state thermodynamic parameters, we can exploit Arrhenius analysis to perform similar temperature-dependent studies for the folding/unfolding rate constants

$$k(T) = A \exp(-\Delta H_{act}/RT) \quad (5)$$

which predicts a linear dependence of $\ln(k(T))$ on $1/T$ with a slope of $-\Delta H_{act}/R$. Sample Arrhenius plots for TLR1 are displayed in Figure S4 for the folding/unfolding rate constant (k_{fold}) at 0, 30, and 50% glycerol concentrations. The raw experimental data in the upper panels of Figure S4 exhibit three parallel lines vertically offset from one another, which is consistent with the activation energy for folding/unfolding being insensitive to an increase in the glycerol concentration. This suggests that the unfolded and folded states of the RNA do not form preferentially differential interactions with glycerol. However, the corresponding pre-exponential factor intercepts [i.e., $\ln(A)$] in Figure S4 do shift significantly with added glycerol, as also expected because of the higher solvent viscosities and longer diffusional time scales associated with an increasing glycerol fraction.

It is important to note, however, that there is also a strong temperature dependence in the solvent viscosity by itself, which we have ignored thus far but for which we can easily make a quantitative correction. From eq 3, we can rewrite the rate constant in terms of thermodynamic parameters of the transition state

$$k_{fold}(T) = \kappa(T)[\omega_{TST}/2\pi] \exp(\Delta S^{\ddagger}/R) \exp(-\Delta H^{\ddagger}/RT) \quad (6)$$

where $\kappa(T)$ is the transmission coefficient, $\Delta H^{\ddagger}$ ($\Delta S^{\ddagger}$) is the barrier enthalpy (entropy), and $\nu_{TST} = \omega_{TST}/2\pi$ is the "attempt" frequency for displacement from the unfolded conformation toward the folding transition state. In the context of Kramers'/Grote–Hynes' theory, this transmission coefficient $\kappa(T)$ will vary strongly with temperature, primarily because of changes in the solvent viscosity, which we can directly take into account by scaling the observed rate constants by $\eta(T)$. Specifically, a plot of $\ln(k_{fold}\eta(T))$ versus $1/T$ is expected to yield a straight line with slope $(-\Delta H^{\ddagger}/R)$ and intercept $(\ln[\mu\omega_{TST}(T)/12\pi^2R] + \Delta S^{\ddagger}/R)$ characterizing the transition-state barrier for folding.

These viscosity-corrected plots are presented in the lower panel of Figure S4, which reveal kinetic data for the TLR1 construct at three glycerol concentrations (0, 30, and 50 v/v %) and all temperatures. The nearly overlapping nature of these curves simply confirms that the transition-state enthalpy for folding/unfolding events is insensitive to the glycerol fraction, that is, $\Delta\Delta H^{\ddagger} \approx$ kcal/mol. A similar behavior is also observed for the van't Hoff plots in Figure S3, which implies an absence of an appreciable differential enthalpic interaction between glycerol and water for unfolded, folded, or transition-state conformations of the three different RNA tertiary constructs. Furthermore, the fact that the corrected curves in Figure S4 (lower panel) become nearly superimposable also indicates that the corresponding entropy differences between the folded/unfolded and transition states must also be insensitive to glycerol content, that is, $\Delta\Delta S^{\ddagger} \approx$ units. Once again, all the single-molecule kinetic results are consistent with Kramers'/Grote–Hynes' theory in the high friction limit, whereby the rate constant for folding/unfolding is dominated by solvent viscosity. Alternatively stated, solvent viscosity directly influences the frequency with which the different conformations of the tetraloop–receptor construct are sampled, but for the ubiquitous tetraloop receptor RNA tertiary interaction, increasing solvent viscosity with glycerol leaves the thermodynamic parameters of the transition-state barrier unchanged.

DOI: 10.1021/acs.jpcb.8b04014
J. Phys. Chem. B 2018, 122, 8796–8804

4. DISCUSSION

4.1. RNA Tertiary Folding is Diffusive. In the previous sections, the viscosity dependence of tetraloop−receptor folding/unfolding kinetics has been analyzed in the context of Kramers' rate theory, which was based on diffusive exploration of conformational space along the reaction coordinate. Because the GAAA tetraloop is connected to the larger 11 nt receptor through a flexible tether [either polymeric (EG_6) or nucleic acid (rU_7, rA_7) based], the folding reaction coordinate can effectively be visualized with reduced dimensionality as slow diffusional sampling of the relative orientation and spatial separation of the tetraloop and its receptor over a physical region limited by the length of the linker. One explicit prediction from Kramers' theory is therefore a $1/\eta$ dependence for both folding and unfolding processes, which is empirically confirmed at the single-molecule level by tuning the solvent viscosity with glycerol, as shown in Figures 4 and 5. Note that while a diffusional approach to the transition state might be easily rationalized as a mechanism for folding, it is less obvious that the unfolding rate constant must also be inversely dependent on solution viscosity. However, a reverse diffusional approach to the unfolding transition state from the folded conformation requires the breaking of many hydrogen bonds formed in the tetraloop−receptor complex. This process requires the tetraloop center of mass to be displaced from the receptor, which from Kramers' theory would provide a natural motivation for the inverse viscosity dependence observed experimentally. We note that this is also in good agreement with model protein studies by Thirumalai and co-workers, which found an inverse dependence of the folding rate constants on the solution friction under high viscosity conditions.[34,35,48]

A second direct prediction of Kramers'/Grote−Hynes' theory is that K_{eq} (and therefore ΔG°) should be invariant with respect to viscosity and thus $\Delta\Delta G^\circ = 0$. This arises simply from the fact that $K_{eq} = k_{fold}/k_{unfold}$, both of which have an identical $1/\eta$ dependence on viscosity (eq 2). Indeed, the data in Figure 5 are in excellent agreement with this prediction, as evident in the ΔG° values plotted in Figures 6 and S1, which are flat, scattered around a single energy value (horizontal gray dashed line) and indicate negligible preferential thermodynamic interaction between glycerol and either the folded or unfolded states.

4.2. Temperature/Viscosity-Dependent RNA Tertiary Folding. We can take this equilibrium analysis one step further by introducing temperature as an independent experimental variable. Specifically, van't Hoff analysis of the temperature-dependent equilibrium data (Figure S3) permits one to independently deconstruct the free energy change (ΔG°) into its enthalpic (ΔH°, slope) and entropic (ΔS°, intercept/R) contributions. There should be no dependence of these thermodynamic parameters on dynamical properties such as viscosity, provided one can neglect preferential interactions between glycerol and the folded and unfolded conformations of the RNA constructs. Indeed, the experimental results are consistent with this expectation, with fits to the data in Figure S4 yielding identical enthalpic changes within experimental uncertainty.

Because the folding/unfolding rate constants change 5−10 fold as a function of glycerol content, it is less obvious from an Arrhenius perspective that the transition-state barrier enthalpies and/or entropies should be similarly viscosity-independent. Indeed, the Arrhenius plots of $\ln(k)$ versus $1/T$ (shown in Figure S4 upper panels) reveal strong parallel shifts downward with increasing glycerol content, which, though still consistent with negligible change in the transition-state enthalpy, could imply a decrease in the transition-state entropy. The simplest explanation for this decrease is that the dynamical effects in a thermodynamic formulation of the transition-state theory are captured in the attempt frequency, $\omega(T)$, which for Kramers' 1D diffusional approach to the transition state varies inversely with solvent viscosity. Indeed, we were able to correct for this exactly by plotting $\ln[k_{fold\ or\ unfold}\eta(T)]$ versus $1/T$, thereby taking into account the strongly activated temperature-dependent viscosity. As seen in Figure S4 (lower panels), the data sets now are essentially superimposable. In other words, the free energy barrier heights ($\Delta G^{\ddagger}_{fold}$ and $\Delta G^{\ddagger}_{unfold}$) in the folding/unfolding direction do not change with increasing viscosity. Instead, the rate processes associated with conformational search and free diffusion to the barrier-crossing region are each slowed equivalently, resulting in a balanced reduction in k_{fold} and k_{unfold}, as experimentally observed in Figures 4 and 5.

4.3. Tertiary RNA Folding at the Viscous "Speed Limit". As alluded to previously, plots of $1/k$ versus η_{solv} can yield more detailed information about the two-state folding process. In the case of the three linkers investigated in this work, the plots in Figure 7 (X = EG_6) and Figure S2 (X = rU_7 and rA_7) each yield straight line fits with intercepts very close to the origin. This result implies that there is no significant contribution to folding kinetics due to internal friction. Although the internal frictional contributions for RNA folding therefore appear to be vanishingly small for all three constructs, the slopes (in cP/s) for the folding/unfolding rate constants do differ significantly (see Figure S2). For the solvent viscosity dependence of the folding rate constant, for example, the reciprocal slope values increase nearly 6-fold between X = EG_6 [26.3(2) cP/s], X = rU_7 [11(3) cP/s] and X = rA_7 [4.6(2) cP/s], where the larger number implies a lower sensitivity to viscogenic effects.

Such trends stand in clear contrast with the unfolding data (see Figure S2), where the kinetic differences between the three linker constructs prove to be less than 30%. The greater similarity in the viscosity-dependent unfolding data suggests that only relatively modest multidimensional diffusion of the GAAA tetraloop and receptor is required to achieve the unfolding transition state. These data are therefore all in agreement with an enthalpically "late", compact transition state for folding (or an "early" transition state for unfolding) with the tetraloop in close proximity to the receptor, yet with few stabilizing interactions formed (or remaining).

As a final observation, instead of probing the viscosity-dependent kinetics of the GAAA tetraloop receptor tertiary interaction in a unimolecular construct, it could in principle be an interesting experimental control to explore the corresponding single-molecule docking/undocking kinetics in a purely bimolecular construct, for example, with a single GAAA tetraloop moiety freely diffusing up to a single tetraloop receptor tethered to the cover slip. Indeed, because the corresponding bimolecular kinetics is likely to proceed via rate constants dominated by diffusion, one might again predict a strong inverse sensitivity to viscosity and thus a linear plot of the docking rate constant k_{dock} versus $1/\eta$ with zero intercept. Unfortunately, this is precisely the same kinetic dependence on

DOI: 10.1021/acs.jpcb.8b04014
J. Phys. Chem. B 2018, 122, 8796−8804

viscosity exhibited by each of the unimolecular GAAA tetraloop receptor constructs, which is what would make it hard in such experiments to distinguish between frictional contributions due to (i) free diffusion of the GAAA tetraloop with respect to the tetraloop receptor and (ii) eventual docking formation of the tertiary motif. In this regard, it is worth noting that the 6-fold differences in slopes cited above (Figure S2) clearly correspond to constructs with an identical tetraloop−receptor interaction. These slopes differences must therefore report only on unimolecular diffusional effects associated with polymeric (EG_6) versus nucleic acid (rU_7 and rA_7) linkers. This corresponds to a sensitivity in the rate constant to viscosity in the decreasing order of $rA_7 > rU_7 > EG_6$, which would be in qualitative agreement with flexibility expectations for nucleic acid versus simple PEG tethering of the tetraloop and receptor. Most importantly, however, the experimental observation (see Figure S2) of a linear dependence on inverse viscosity with near zero intercept for each of these linkers makes it clear that the folding rates can get very large at sufficiently low viscosities. We thus conclude that the current body of smFRET data supports a paradigm for folding of the GAAA tetraloop receptor tertiary interaction motif at the viscous "speed limit."

5. SUMMARY AND CONCLUSIONS

In this work, we have used smFRET to measure the folding kinetics of a ubiquitous RNA structural motif as a function of solvent viscosity (η_{solv}). The results are fully consistent with Kramers'/Grote−Hynes' theory for diffusion rate-limited crossing over an effective 1D transition state barrier. Such treatments predict the rate constants for both folding/unfolding to vary inversely with η_{solv}, as experimentally observed, but with transition-state enthalpies, entropies, and free energies insensitive to η_{solv}, which we also observe. We consider the effects of an additional intrinsic viscosity ($\eta_{eff} = \eta_{solv} + \eta_{int}$), which could arise due to roughness in the free energy surface. Plots of $k_{fold\ or\ unfold}$ versus η_{solv} reveal that the GAAA tetraloop−receptor exhibits negligibly small intrinsic viscosities ($\eta_{int} \approx 0.1(2)$ cP) relative to cellular viscosities ($\eta_{solv} > 1.0$ cP). The folding rate constants exhibit a viscosity dependence that is sensitive to the linker composition (X = EG_6, rU_7, or rA_7), which suggests that folding process includes not only diffusion of the GAAA tetraloop−receptor moiety but also conformational search in the polymeric or nucleic acid linker. By way of contrast, the relative insensitivity of the viscosity dependence of the unfolding rate constants to linker composition suggests that much smaller scale conformational changes involving only the GAAA tetraloop and receptor are necessary to access the unfolding transition state. Finally, the small values of intrinsic viscosity [$\eta_{int} \approx 0.1(2)$ cP] compared to typical cellular values ($\eta_{solv} > 1.0$ cP) imply that the folding/unfolding kinetics of modular RNA tertiary interactions are fully limited by solvent viscosity and take place at the viscous "speed limit." Similar linear plots of $k_{fold\ or\ unfold}$ versus $1/\eta$ with near zero intercepts have been obtained for both flexible polymer (EG_6) as well as more biochemically relevant nucleic acid linkers (rU_7 and rA_7). The results provide valuable additional support for a negligible contribution from internal friction effects in the binding of the ubiquitous GAAA tetraloop receptor tertiary motif itself.

■ ASSOCIATED CONTENT

Supporting Information

The Supporting Information is available free of charge on the ACS Publications website at DOI: 10.1021/acs.jpcb.8b04014.

Four additional plots of the viscosity and temperature dependence of the folding/unfolding rate constants; viscosity dependence of the rate and equilibrium constants for folding and unfolding of the RNA constructs with each of the three linkers; plot of $1/k$ (in s) versus η (in cP) for each of the three flexible linkers (X = EG_6, rU_7, and rA_7), sample van't Hoff plot of $R\ \ln\{K_{eq}\}$ versus $1/T$ for the TLR1 construct, and Arrhenius plots of $\ln\{k\}$ and $\ln\{k \times \eta\}$ for the RNA folding/unfolding rate constants versus $1/T$ (PDF)

■ AUTHOR INFORMATION

Corresponding Author

*E-mail: djn@jila.colorado.edu.

ORCID

David J. Nesbitt: 0000-0001-5365-1120

Notes

The authors declare no competing financial interest.

■ ACKNOWLEDGMENTS

Funding for this work was provided by the National Science Foundation (CHE-1665271, PHY-1734006) and the National Institute for Standards and Technology. N.F.D. would like to acknowledge postdoctoral fellowship support from the National Research Council and E.D.H. received funding from the National Institutes of Health Molecular Biophysics Training Grant (T32 GM-065103).

■ REFERENCES

(1) Medalia, O.; Weber, I.; Frangakis, A. S.; Nicastro, D.; Gerisch, G.; Baumeister, W. Macromolecular Architecture in Eukaryotic Cells Visualized by Cryoelectron Tomography. *Science* **2002**, *298*, 1209−1213.

(2) Clegg, J. S. Properties and Metabolism of the Aqueous Cytoplasm and Its Boundaries. *Am. J. Physiol.* **1984**, *246*, R133−R151.

(3) Sear, R. P. The Cytoplasm of Living Cells: A Functional Mixture of Thousands of Components. *J. Phys.: Condens. Matter* **2005**, *17*, S3587−S3595.

(4) Chung, H. S.; Piana-Agostinetti, S.; Shaw, D. E.; Eaton, W. A. Structural Origin of Slow Diffusion in Protein Folding. *Science* **2015**, *349*, 1504−1510.

(5) Soranno, A.; Buchli, B.; Nettels, D.; Cheng, R. R.; Muller-Spath, S.; Pfeil, S. H.; Hoffmann, A.; Lipman, E. A.; Makarov, D. E.; Schuler, B. Quantifying Internal Friction in Unfolded and Intrinsically Disordered Proteins with Single-Molecule Spectroscopy. *Proc. Natl. Acad. Sci. U.S.A.* **2012**, *109*, 17800−17806.

(6) Borgia, A.; Wensley, B. G.; Soranno, A.; Nettels, D.; Borgia, M. B.; Hoffmann, A.; Pfeil, S. H.; Lipman, E. A.; Clarke, J.; Schuler, B. Localizing Internal Friction Along the Reaction Coordinate of Protein Folding by Combining Ensemble and Single-Molecule Fluorescence Spectroscopy. *Nat. Commun.* **2012**, *3*, 1195.

(7) Cellmer, T.; Henry, E. R.; Hofrichter, J.; Eaton, W. A. Measuring Internal Friction of an Ultrafast-Folding Protein. *Proc. Natl. Acad. Sci. U.S.A.* **2008**, *105*, 18320−18325.

(8) Liu, F.; Nakaema, M.; Gruebele, M. The Transition State Transit Time of Ww Domain Folding Is Controlled by Energy Landscape Roughness. *J. Chem. Phys.* **2009**, *131*, 195101.

(9) Hagen, S. J. Solvent Viscosity and Friction in Protein Folding Dynamics. *Curr. Protein Pept. Sci.* **2010**, *11*, 385−395.

DOI: 10.1021/acs.jpcb.8b04014
J. Phys. Chem. B 2018, 122, 8796−8804

(10) Wensley, B. G.; Batey, S.; Bone, F. A. C.; Chan, Z. M.; Tumelty, N. R.; Steward, A.; Kwa, L. G.; Borgia, A.; Clarke, J. Experimental Evidence for a Frustrated Energy Landscape in a Three-Helix-Bundle Protein Family. *Nature* **2010**, *463*, 685.
(11) Jas, G. S.; Eaton, W. A.; Hofrichter, J. Effect of Viscosity on the Kinetics of Alpha-Helix and Beta-Hairpin Formation. *J. Phys. Chem. B* **2001**, *105*, 261−272.
(12) Dumont, C.; Emilsson, T.; Gruebele, M. Reaching the Protein Folding Speed Limit with Large, Sub-Microsecond Pressure Jumps. *Nat. Methods* **2009**, *6*, 515.
(13) Gruebele, M. Downhill Protein Folding: Evolution Meets Physics. *C. R. Biol.* **2005**, *328*, 701−712.
(14) Yang, W. Y.; Gruebele, M. Folding at the Speed Limit. *Nature* **2003**, *423*, 193−197.
(15) Nguyen, H.; Jäger, M.; Kelly, J. W.; Gruebele, M. Engineering Beta-Sheet Protein toward the Folding Speed Limit. *J. Phys. Chem. B* **2005**, *109*, 15182−15186.
(16) Portman, J. J.; Takada, S.; Wolynes, P. G. Microscopic Theory of Protein Folding Rates. Ii. Local Reaction Coordinates and Chain Dynamics. *J. Chem. Phys.* **2001**, *114*, 5082−5096.
(17) Hyeon, C.; Thirumalai, D. Chain Length Determines the Folding Rates of RNA (Vol 102, Pg L11, 2012). *Biophys. J.* **2012**, *102*, 1235.
(18) Kramers, H. A. Brownian Motion in a Field of Force and the Diffusion Model of Chemical Reactions. *Physica* **1940**, *7*, 284−304.
(19) Grote, R. F.; Hynes, J. T. The Stable States Picture of Chemical-Reactions. 2. Rate Constants for Condensed and Gas-Phase Reaction Models. *J. Chem. Phys.* **1980**, *73*, 2715−2732.
(20) Grote, R. F.; Hynes, J. T. Reactive Modes in Condensed Phase Reactions. *J. Chem. Phys.* **1981**, *74*, 4465−4475.
(21) Grote, R. F.; Hynes, J. T. Energy Diffusion-Controlled Reactions in Solution. *J. Chem. Phys.* **1982**, *77*, 3736−3743.
(22) Grote, R. F.; Van der Zwan, G.; Hynes, J. T. Frequency-Dependent Friction and Solution Reaction-Rates. *J. Phys. Chem.* **1984**, *88*, 4676−4684.
(23) Northrup, S. H.; Hynes, J. T. The Stable States Picture of Chemical-Reactions .1. Formulation for Rate Constants and Initial Condition Effects. *J. Chem. Phys.* **1980**, *73*, 2700−2714.
(24) Hänggi, P.; Talkner, P.; Borkovec, M. Reaction-Rate Theory - 50 Years after Kramers. *Rev. Mod. Phys.* **1990**, *62*, 251−341.
(25) Ansari, A.; Jones, C. M.; Henry, E. R.; Hofrichter, J.; Eaton, W. A. The Role of Solvent Viscosity in the Dynamics of Protein Conformational-Changes. *Science* **1992**, *256*, 1796−1798.
(26) Chung, H. S.; Eaton, W. A. Single-Molecule Fluorescence Probes Dynamics of Barrier Crossing. *Nature* **2013**, *502*, 685.
(27) Berezhkovskii, A. M.; Szabo, A.; Weiss, G. H.; Zhou, H.-X. Reaction Dynamics on a Thermally Fluctuating Potential. *J. Chem. Phys.* **1999**, *111*, 9952−9957.
(28) Chung, H. S.; Gopich, I. V. Fast Single-Molecule FRET Spectroscopy: Theory and Experiment. *Phys. Chem. Chem. Phys.* **2014**, *16*, 18644−18657.
(29) Chung, H. S.; Gopich, I. V.; McHale, K.; Cellmer, T.; Louis, J. M.; Eaton, W. A. Extracting Rate Coefficients from Single-Molecule Photon Trajectories and FRET Efficiency Histograms for a Fast-Folding Protein. *J. Phys. Chem. A* **2011**, *115*, 3642−3656.
(30) Chung, H. S.; Louis, J. M.; Eaton, W. A. Experimental Determination of Upper Bound for Transition Path Times in Protein Folding from Single-Molecule Photon-by-Photon Trajectories. *Proc. Natl. Acad. Sci. U.S.A.* **2009**, *106*, 11837−11844.
(31) Gopich, I. V.; Szabo, A. Decoding the Pattern of Photon Colors in Single-Molecule FRET. *J. Phys. Chem. B* **2009**, *113*, 10965−10973.
(32) Soranno, A.; Koenig, I.; Borgia, M. B.; Hofmann, H.; Zosel, F.; Nettels, D.; Schuler, B. Single-Molecule Spectroscopy Reveals Polymer Effects of Disordered Proteins in Crowded Environments. *Proc. Natl. Acad. Sci. U.S.A.* **2014**, *111*, 4874−4879.
(33) Yang, W. Y.; Gruebele, M. Folding Lambda-Repressor at Its Speed Limit. *Biophys. J.* **2004**, *87*, 596−608.
(34) Klimov, D. K.; Thirumalai, D. Viscosity Dependence of the Folding Rates of Proteins. *Phys. Rev. Lett.* **1997**, *79*, 317−320.
(35) Thirumalai, D. Time Scales for the Formation of the Most Probable Tertiary Contacts in Proteins with Applications to Cytochrome C. *J. Phys. Chem. B* **1999**, *103*, 608−610.
(36) Thirumalai, D.; Woodson, S. A. Kinetics of Folding of Proteins and RNA. *Acc. Chem. Res.* **1996**, *29*, 433−439.
(37) Plaxco, K. W.; Baker, D. Limited Internal Friction in the Rate-Limiting Step of a Two-State Protein Folding Reaction. *Proc. Natl. Acad. Sci. U.S.A.* **1998**, *95*, 13591−13596.
(38) Hodak, J. H.; Fiore, J. L.; Nesbitt, D. J.; Downey, C. D.; Pardi, A. Docking Kinetics and Equilibrium of a GAAA Tetraloop-Receptor Motif Probed by Single-Molecule FRET. *Proc. Natl. Acad. Sci. U.S.A.* **2005**, *102*, 10505.
(39) Fiore, J. L.; Hodak, J. H.; Piestert, O.; Downey, C. D.; Nesbitt, D. J. Monovalent and Divalent Promoted GAAA Tetraloop-Receptor Tertiary Interactions from Freely Diffusing Single-Molecule Studies. *Biophys. J.* **2008**, *95*, 3892−3905.
(40) Holmstrom, E. D.; Nesbitt, D. J. Real-Time Infrared Overtone Laser Control of Temperature in Picoliter H_2O Samples: "Nano-bathtubs" for Single Molecule Microscopy. *J. Phys. Chem. Lett.* **2010**, *1*, 2264−2268.
(41) Fiore, J. L.; Kraemer, B.; Koberling, F.; Edmann, R.; Nesbitt, D. J. Enthalpy-Driven RNA Folding: Single-Molecule Thermodynamics of Tetraloop-Receptor Tertiary Interaction. *Biochemistry* **2009**, *48*, 2550−2558.
(42) Fiore, J. L.; Holmstrom, E. D.; Fiegland, L. R.; Hodak, J. H.; Nesbitt, D. J. The Role of Counterion Valence and Size in GAAA Tetraloop-Receptor Docking/Undocking Kinetics. *J. Mol. Biol.* **2012**, *423*, 198−216.
(43) Holmstrom, E. D.; Fiore, J. L.; Nesbitt, D. J. Thermodynamic Origins of Monovalent Facilitated RNA Folding. *Biochemistry* **2012**, *51*, 3732−3743.
(44) Downey, C. D.; Fiore, J. L.; Stoddard, C. D.; Hodak, J. H.; Nesbitt, D. J.; Pardi, A. Metal Ion Dependence, Thermodynamics, and Kinetics for Intramolecular Docking of a GAAA Tetraloop and Receptor Connected by a Flexible Linker. *Biochemistry* **2006**, *45*, 3664−3673.
(45) Fiore, J. L.; Holmstrom, E. D.; Nesbitt, D. J. Entropic Origin of Mg2+-Facilitated RNA Folding. *Proc. Natl. Acad. Sci. U.S.A.* **2012**, *109*, 2902−2907.
(46) Segur, J. B.; Oberstar, H. E. Viscosity of Glycerol and Its Aqueous Solutions. *Ind. Eng. Chem.* **1951**, *43*, 2117−2120.
(47) Dupuis, N. F.; Holmstrom, E. D.; Nesbitt, D. J. Molecular-Crowding Effects on Single-Molecule RNA Folding/Unfolding Thermodynamics and Kinetics. *Proc. Natl. Acad. Sci. U.S.A.* **2014**, *111*, 8464−8469.
(48) Thirumalai, D.; Woodson, S. A. Maximizing RNA Folding Rates: A Balancing Act. *RNA* **2000**, *6*, 790−794.

DOI: 10.1021/acs.jpcb.8b04014
J. Phys. Chem. B 2018, 122, 8796−8804